Implementation of boundary conditions for locked waves

Report submitted to RIKZ
(Project RKZ-410)

H.A.H. Petit
J.A. Battjes

Report XX-01
November 2001

Delft University of Technology
Faculty of Civil Engineering and Geosciences
Fluid Mechanics Section

Contents

List of Figures

1 Introduction

This report refers to the work done at the Fluid Mechanics Section within the framework of the Netherlands Centre for Coastal Research (NCK). As shown by Reniers et al. (2000) there are strong indications that wave-group related phenomena are important in the development of rip channels. It is to be expected that edge waves caused by wave-group induced long waves can be of significant influence on the development of the bathymetry and shoreline.

In the development of research models for morphodynamic evolution in the coastal zone the first step is an accurate description of the flow field. In this project use is made of the Delft3D-flow solver to model waves at the scale of wave groups in the coastal zone. The Delft3D model was originally developed to model tide induced flow in sea, coast and estuaries. In this project we use the version of the model which uses the depth averaged flow option. For the boundary conditions used in a model intended for time scales corresponding with tidal flow the demands are not very high. The waves modelled by such models are extremely long and the phase changes along the open boundaries of the model very small. The Delft3D program therefore had a simplified version of the Riemann boundary conditions, effectively using the assumption that outgoing waves at the boundary were travelling perpendicularly to the boundary. On a time and space scale of wave groups this assumption proves to be insufficient as shown in Petit et al. (2000). A program not equipped with boundary conditions that allow both locked and free waves to enter the domain and free waves to leave the domain without significant (non-physical) reflections, cannot be used for modeling long waves in the coastal zone accurately. It was shown that the Riemann boundary conditions developed by Van Dongeren and Svendsen (1997) could very well offer a solution to this problem. Tests with a simplified model then showed that these boundary conditions indeed performed very well.

In the simplified test model use was made of prescribed wave forces. These were not related to numerically determined carrier wave densities. In the Delft3D adaptions, the wave forces are determined as minus the divergence of the radiation-stress tensor. This involves numerical differentiation of (multiples of) the carrier-wave energy. One of the problems encountered in making the Delft3D program suitable for the simulation of short wave induced flow proved the determination of the wave forces near weakly reflective boundaries.

This report describes a number of one-dimensional test cases used to locate the problems of the numerical approach. For one problem, regarding the numerical determination of the wave forces near the boundary, a solution was found by using extrapolation and by using a different discretization for the transport of wave energy near the boundary.

Unfortunately not all of the problems were solved, but they have to be tackled one at a time!

2 Free waves

The implemented boundary conditions were developed such that both locked and free waves can be used as input for the model. They have the limitation that locked waves cannot be exported from the model. In a previous report ('Modified boundary conditions and field equations for a 2D surf beat model', report 03-01, June 2001) it was already reported that free waves could traverse a modelled region quite well. The reflections depended on the exit-angle and were shown to be acceptable. In the one-dimensional test case described in section 3 of this report, locked waves are used as input for the model and free waves exit the model at the same boundary. In order to warrant that free waves are treated correctly by the model, we repeated the test for a simple one-dimensional case, which corresponds with the test used in section 3.

2.1 Test case

In this test we send in a free long wave at the left boundary and use a closed boundary at the right side of the model. The resulting standing wave should have twice the amplitude of the incoming wave. Two separate cases were considered. In case 1 the wave length was equal to the length of the domain, resulting in an anti-node of the free surface elevation at the left boundary. At this boundary the velocity should be zero. In case 2 the wave length was chosen to be 4/3 of the length of the domain, resulting in a node of the free surface elevation at the left boundary. The parameters used in the computation were: L=200 m (the length of the domain modelled in the computation) and H=8 m (the constant depth value). For case 1 we used the frequency f=0.043837 Hz (the frequency of the incoming wave), yielding λ=200 m. For case 2 we used the frequency f=0.033026 Hz, yielding λ=266.666 m. For both cases the amplitude of the incoming waves was chosen: ζ=0.01 m. The numerical parameters were: Δx=5 m and Δt=1.2 s. In Figures 1(a) and 1(b) we show $\frac{1}{2}\left(\max(\zeta; t_0 \leq t \leq t_1) - \min(\zeta; t_0 \leq t \leq t_1)\right)$, which is the envelope of the resulting standing wave. The parameter t_0 was chosen large enough to disregard the incoming tapered signal so that only the standing wave is present in the considered time interval. The parameter t_1 indicates the end of the computation. The index along the horizontal axis of the figures gives the number of the cell in the computational grid. The first active cell has number 2. The last active cell has number 40.

As can be seen from the results of these tests, the free surface elevation assumes the expected values. The maximum value for the envelope of case 1 is found to be 0.0199, for case 2 this value becomes 0.0201.

3 Locked waves

The numerical modelling of locked waves proves to be not a trivial matter. One of the reasons for this can be found in the fact that numerical differentiation is not an accurate process. Since the wave force is modelled as minus the divergence of the radiation-stress tensor (which is linearly dependent of the wave energy), numerical differentiation cannot be avoided. The test described in the following sub-section will reveal that the numerical inaccuracies can easily become dominant.

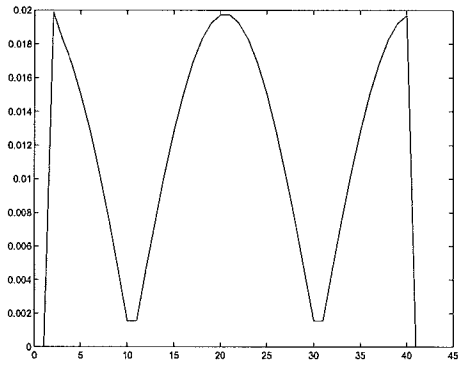

(a) Free surface envelope: case 1

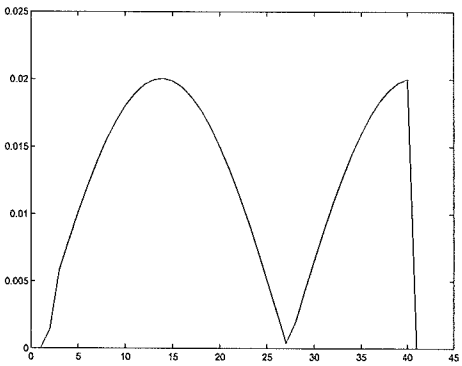

(b) Free surface envelope: case 2

Figure 1: Standing free waves

3.1 Test case

In order to assess whether the boundary conditions perform adequately, we made use of a simple test case of which the analytical solution is known. The test case is one-dimensional and can thus only reveal some of the possible shortcomings of the discretization. It is the purpose of this test to send in a locked wave at the left boundary. This is realized by choosing a combination of a prescribed elevation and the corresponding (carrier-wave) energy signal. The locked wave is transported with the energy field, which travels with the group velocity towards the closed right boundary. At this boundary we assume that all of the carrier-wave energy is dissipated. It can be thought of as a very steep slope on which all carrier waves break. Here this is modelled by allowing the energy to leave the domain at this right boundary. The boundary is thus transparent for the carrier-wave energy. For the long waves the boundary is closed, acting as a wall where the normal velocity is zero. The resulting flow field will be that of a right-going locked wave and a left-going free wave. The amplitude of the free wave is determined by the boundary condition at the wall ($u = 0$), where it has to cancel the velocity contribution of the locked wave.

The domain extends from $x = 0$ to $x = L$. At the left boundary we have a bi-chromatic signal with frequencies ω_1 and ω_2 of which the energy density is prescribed at the boundary. It is transported inward with the group velocity C_g. The divergence of the radiation stress describes the wave force, which causes a bound wave to follow the inward travelling energy fluctuations. Since the energy is transported through the right boundary the locked wave is still forced there. The two wave signals (carrier waves), which enter at the left boundary, are given by:

$$\zeta_1 = A_1 \exp(k_1 x - \omega_1 t) \ , \ \zeta_2 = A_2 \exp(k_2 x - \omega_2 t) \tag{1}$$

Note that these waves are not modelled in the program, their energy however, is. The carrier-wave energy is found as:

$$E = \frac{1}{2}\rho g \zeta \zeta^* = \frac{1}{2}\rho g \left(A_1^2 + A_2^2 + 2A_1 A_2 \cos\left((k_1 - k_2)x - (\omega_1 - \omega_2)t\right)\right) =$$

$$\frac{1}{2}\rho g\left(A_1^2+A_2^2+2A_1A_2\cos\left((k_1-k_2)\left(x-\frac{\omega_1-\omega_2}{k_1-k_2}t\right)\right)\right)\approx$$
$$\frac{1}{2}\rho g\left(A_1^2+A_2^2+2A_1A_2\cos\left((k_1-k_2)(x-C_gt)\right)\right). \tag{2}$$

The radiation stress is (in this one dimensional case) given by:

$$S=\left(2\frac{C_g}{C}-\frac{1}{2}\right)E. \tag{3}$$

The linearized equations for momentum and mass conservation are given by:

$$\frac{\partial u}{\partial t}+g\frac{\partial\zeta}{\partial x}=\frac{-1}{\rho H}\frac{\partial S}{\partial x} \tag{4}$$

and

$$\frac{\partial\zeta}{\partial t}+H\frac{\partial u}{\partial x}=0 \tag{5}$$

respectively.

In the absence of incoming free waves, the solution of these equations can be given as the sum of right-going bound waves and left-going free waves. For the bound waves the velocity and free surface elevation are given by:

$$u_b=\frac{C_g}{gH-C_g^2}F_x\left(x-C_gt\right) \tag{6}$$

and

$$\zeta_b=\frac{H}{gH-C_g^2}F_x\left(x-C_gt\right). \tag{7}$$

For the free waves these become:

$$u_f=\frac{-C_g}{gH-C_g^2}F_x\left(\left(1+\frac{C_g}{\sqrt{gH}}\right)L-\frac{C_g}{\sqrt{gH}}\left(x-\sqrt{gH}t\right)\right) \tag{8}$$

and

$$\zeta_f=\sqrt{\frac{H}{g}}\frac{C_g}{gH-C_g^2}F_x\left(\left(1+\frac{C_g}{\sqrt{gH}}\right)L-\frac{C_g}{\sqrt{gH}}\left(x-\sqrt{gH}t\right)\right). \tag{9}$$

In these equations we use the function

$$F_x(\xi)=-\left(2\frac{C_g}{C}-\frac{1}{2}\right)\frac{g}{H}A_1A_2\cos((k_1-k_2)\xi).$$

It is the (zero time average) primitive of $\partial S/\partial x$ multiplied with $\frac{-1}{\rho H}$. For the total free-surface elevation we thus find:

$$\zeta(x,t)=\frac{H}{gH-C_g^2}\left(F_x(x-C_gt)+\frac{C_g}{\sqrt{gH}}F_x\left(\left(1+\frac{C_g}{\sqrt{gH}}\right)L-\frac{C_g}{\sqrt{gH}}\left(x-\sqrt{gH}t\right)\right)\right). \tag{10}$$

3.2 Wave forces

Based on the analysis of the previous section we choose the following parameters for the bi-chromatic wave:

$$f_1 = 0.195\ Hz\ ,\ A_1 = 0.11\ m.$$

$$f_1 = 0.205\ Hz\ ,\ A_1 = 0.09\ m.$$

In the numerical model we used the parameters Δx=5 m and Δt=1.2 s. Based on the average frequency we find a group velocity of C_g=4.619 m/s which implies a CFL number of $C_g \Delta t/\Delta x = 1.108$ for the transport of short-wave energy. The number of discretization points per wave length is given by $2\pi/(\|k_1 - k_2\|\Delta x) = 92.4$. Here k_1 and k_2 are the wave numbers of the incoming carrier waves.

We exported the carrier-wave energy as a function of grid number in x direction after simulating 400 time steps. The result is shown in Figure 2. Since the location of the velocity points and the water-level points are in a staggered arrangement a central discretization is used to determine the derivative to x of the energy. Note that this is a fixed multiple of the wave force since the depth is considered constant in this test. The derivative to x of the energy is presented in Figure 3. The resulting wave force thus shows sudden jumps in value near the left boundary and near the right boundary. In using the weakly reflective boundary conditions the wave force at the left boundary is used to determine the free surface elevation and the velocity there. These forces are thus needed for the weakly reflective boundary conditions to perform well in the case of incoming locked waves and outgoing free waves. Disturbances as found here will cause spurious incoming free waves to be generated at the boundary.

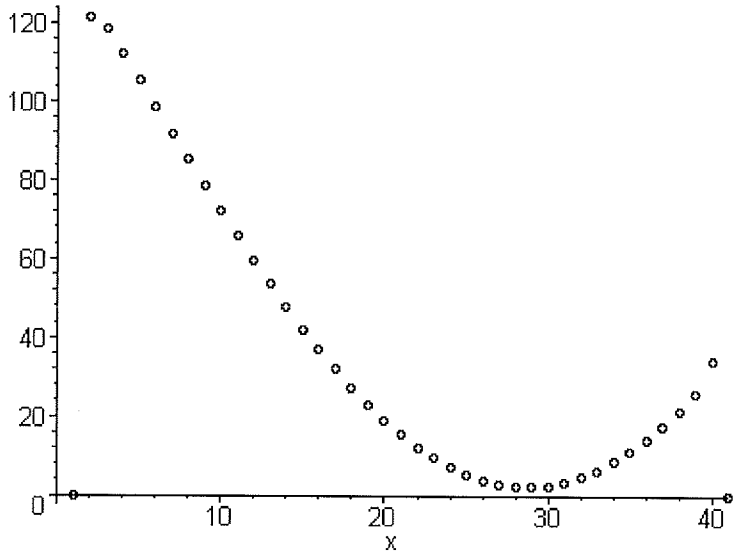

Figure 2: Carrier wave energy as a function of $x/\Delta x$.

The jumps in the derivative of the energy function are caused by the discretization of the energy-transport equation near the boundaries.

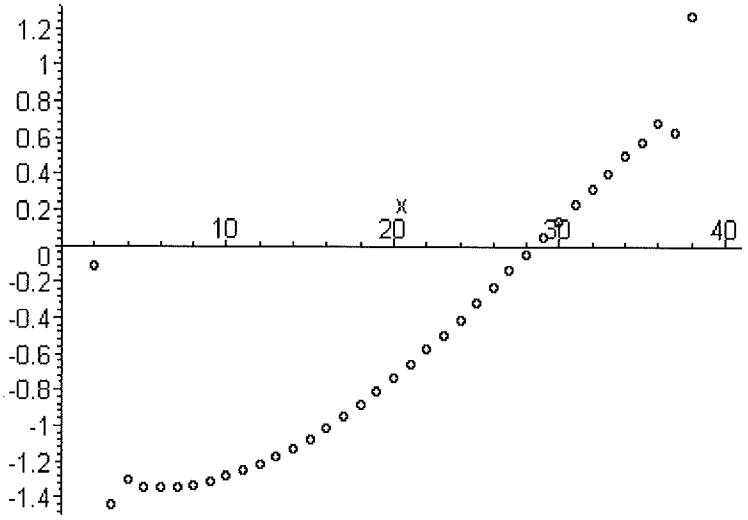

Figure 3: The derivative of the energy as a function of $x/\Delta x$.

3.3 Energy transport

In the simple case studied here the equation to be solved (by the subroutine DIFUWE in Delft3D) is given by:

$$\frac{\partial E}{\partial t} + C_g \frac{\partial E}{\partial x} = 0 \tag{11}$$

where C_g is a positive constant. In the one-dimensional case considered here, the numerical scheme to solve this equation consists of two parts. First an implicit discretization is used for the first half time step. In the second half time step an explicit scheme is used. Near the boundary the problems are caused by both half time steps. In the first half time step use is made of an upwind interpolation to determine the flux through cell boundaries left and right of the location where the new value for the energy is to be determined. The amount fluxed in half a time step is retrieved from the donor cell and attributed to the acceptor cell. The purpose of this procedure is to avoid the loss of energy or the creation of energy in the domain. In order to determine the flux at a cell boundary, three locations for the energy are used, two of which are located upwind from the cell position. As the method is implicit this results in an equation relating these energy values. At some distance from the boundary the resulting equation becomes:

$$\left(1 + \frac{5}{6}\mu\right) E_m^{q+\frac{1}{2}} - \frac{7}{6}\mu E_{m-1}^{q+\frac{1}{2}} + \frac{2}{6}\mu E_{m-2}^{q+\frac{1}{2}} = E_m^q. \tag{12}$$

Here we used for the CFL number $\mu = C_g \Delta t/\Delta x$. This discretization effectively solves the following equation:

$$\frac{\partial E}{\partial t} + C_g \frac{\partial E}{\partial x} = \frac{1}{2} C_g \Delta x (\mu - \frac{1}{3}) \frac{\partial^2 E}{\partial x^2} + O(\Delta x^2). \tag{13}$$

It is thus consistent with the differential equation we want to solve. For the first point at the right of the boundary use is made of a scheme which uses fewer upwind points, simply

because the energy is not defined there. The only upwind information used is taken from the location just left of the boundary where the Dirichlet condition is provided. The scheme used is given by:

$$(1+\frac{3}{4}\mu)E_3^{q+\frac{1}{2}} - \frac{3}{4}\mu E_2^{q+\frac{1}{2}} = E_3^q. \tag{14}$$

This scheme is inconsistent with the equation we want to solve as it effectively discretizes:

$$\frac{\partial E}{\partial t} + \frac{3}{4}C_g\frac{\partial E}{\partial x} = O(\Delta x). \tag{15}$$

In the second half time step of the procedure an explicit discretization is used. At some distance from the boundary this discretization is Central Space Forward Time:

$$E_m^{q+1} = E_m^{q+\frac{1}{2}} - \frac{1}{4}\mu\left(E_{m+1}^{q+\frac{1}{2}} - E_{m-1}^{q+\frac{1}{2}}\right). \tag{16}$$

This step is again consistent as it solves the following differential equation:

$$\frac{\partial E}{\partial t} + C_g\frac{\partial E}{\partial x} = -\frac{1}{4}C_g\mu\Delta x\frac{\partial^2 E}{\partial x^2} + O(\Delta x^2). \tag{17}$$

At the first location right of the boundary however the discretization becomes:

$$E_3^{q+1} = \frac{1}{2}\mu E_2^{q+\frac{1}{2}} + \left(1-\frac{1}{4}\mu\right)E_3^{q+\frac{1}{2}} - \frac{1}{2}\mu E_4^{q+\frac{1}{2}}. \tag{18}$$

This discretization is inconsistent with the equation we want to solve as it effectively discretizes:

$$\frac{\partial E}{\partial t} + \frac{3}{4}C_g\frac{\partial E}{\partial x} = O(\Delta x). \tag{19}$$

By replacing the discretizations near the boundary with consistent discretizations we may give up conservation but expect a smoother result. For the implicit first half time step, the new discretization at the left boundary is now given by:

$$\left(1+\frac{1}{2}\mu\right)E_3^{q+\frac{1}{2}} - \frac{1}{2}\mu E_2^{q+\frac{1}{2}} = E_3^q. \tag{20}$$

For the second half time step the explicit discretization becomes

$$E_3^{q+1} = \left(1-\frac{1}{2}\mu\right)E_3^{q+\frac{1}{2}} + \frac{1}{2}\mu E_2^{q+\frac{1}{2}}. \tag{21}$$

The results using these discretizations are given in Figures 4 and 5. We find that at the left boundary there is still a jump in the derivative (Figure 5). It seems to be located at the boundary however. In the rest of the field the derivative is smoother then using the original discretization. Note that the jumps in the wave energy (Figure 4) are outside the domain of interest as central discretizations are used to determine the derivatives $(\partial E/\partial x|_2 \approx (E_3 - E_2)/\Delta x)$.

Results after other numbers of time steps show a similar behaviour.

If we do not discretize the derivative of the energy at the left boundary directly but determine the wave force by using extrapolation to the boundary, a smooth wave-force field is attained.

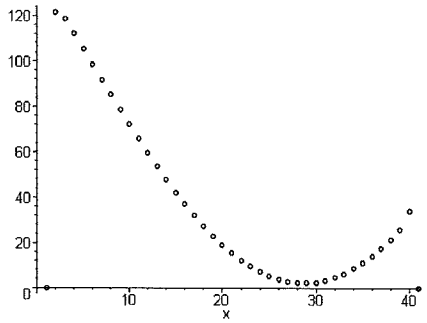

Figure 4: Carrier wave energy discretized with alternative scheme

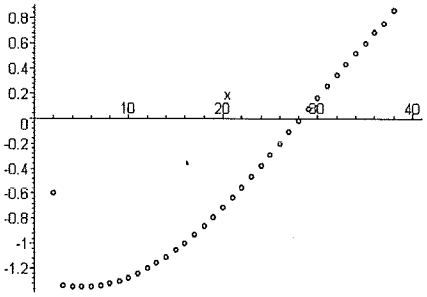

Figure 5: The centrally discretized derivative of the energy

The result using a linear least square approximation based on values in three points in the field is (in the case of an equidistant grid) given by:

$$f_2 = \frac{1}{3}\left(4f_3 + f_4 - 2f_5\right). \tag{22}$$

Here f indicates the wave force devided by ρH. The resulting approximating derivative of the wave energy is shown in Figure 6. Note that the first location at the left of the domain where a wave force is required has index 2. It is the wave force that is used in the weakly reflective boundary condition at the left boundary. In equation(23)in the next section (giving the weakly reflective boundary condition for the first half time step) the wave force devided by ρH is indicated by $f_{x,2,n}^{q+\frac{1}{2}}$.

4 Test results

The test case given in section 3.1 was used to determine if the incoming locked wave is modelled correctly using the described method. The weakly reflective boundary conditions used at the boundary were already described in previous reports Petit et al. (2000) and Petit et al. (2001).We will therefore just repeat them. In the implicit part of the discretization the velocity component in the x-direction is eliminated from the boundary condition yielding:

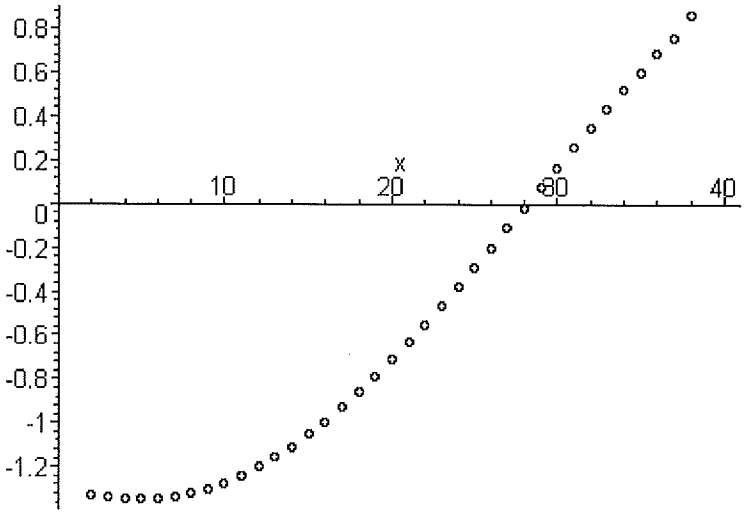

Figure 6: Extrapolated derivative at the boundary

$$\left(\cos(\theta_r)\Delta x + \sqrt{gH}\Delta t\right)\zeta_{2,n}^{q+\frac{1}{2}} + \left(\cos(\theta_r)\Delta_x - \sqrt{gH}\Delta t\right)\zeta_{3,n}^{q+\frac{1}{2}} =$$
$$2\zeta_i^{q+\frac{1}{2}}\Delta x\left(\cos(\theta_r)+\cos(\theta_i)\right) + 2\zeta_b^{q+\frac{1}{2}}\Delta x\left(\cos(\theta_r)+\frac{C_g}{C}\cos(\theta_b)\right) +$$
$$-2\sqrt{\frac{H}{g}}\Delta x u_{2,n}^{q} - \sqrt{\frac{H}{g}}\cos(\theta_r) f_{x,2,n}^{q+\frac{1}{2}}\Delta x\Delta t. \tag{23}$$

In the explicit part:

$$u_{2,j}^{q+1} + \frac{1}{2}\sqrt{\frac{g}{H}}\cos(\theta_r)\left(\zeta_{2,n}^{q+\frac{1}{2}} + \zeta_{3,n}^{q+\frac{1}{2}}\right) =$$
$$\sqrt{\frac{g}{H}}\left(\cos(\theta_r)+\cos(\theta_i)\right)\zeta_i^{q+\frac{1}{2}} + \sqrt{\frac{g}{H}}\left(\cos(\theta_r)+\frac{C_g}{C}\cos(\theta_b)\right)\zeta_b^{q+\frac{1}{2}}. \tag{24}$$

In equation(23) use is made of the wave force at the boundary. It determines the locked wave at the boundary. In equations (23) and (24) we use the subscript 'i' for incoming free waves, the subscript 'b' for incoming bound waves and the subscript 'r' for reflected free waves. The angles indicated with θ are relative to the normal direction at the boundary. This normal direction is outward for the reflected waves and inward for the incoming waves. In the test case studied here all θ's are zero as the problem is one-dimensional, and $\zeta_i = 0$ as no free waves are sent in.

In the last sections attention was paid to the properties of the carrier-wave-energy field and the manipulations needed to extract wave forces from this field. After using the operations needed to smoothen the wave-force field we can now determine the resulting wave motion. We chose to compare the envelope of the free surface elevation of the analytical solution provided in section 3.1 equation (10). In Figures 7(a) and 7(b) we show these results. In the left panel the analytical solution is provided, the right panel gives the numerical result. Note that in the right panel the unit along the x-axes is 5 m.

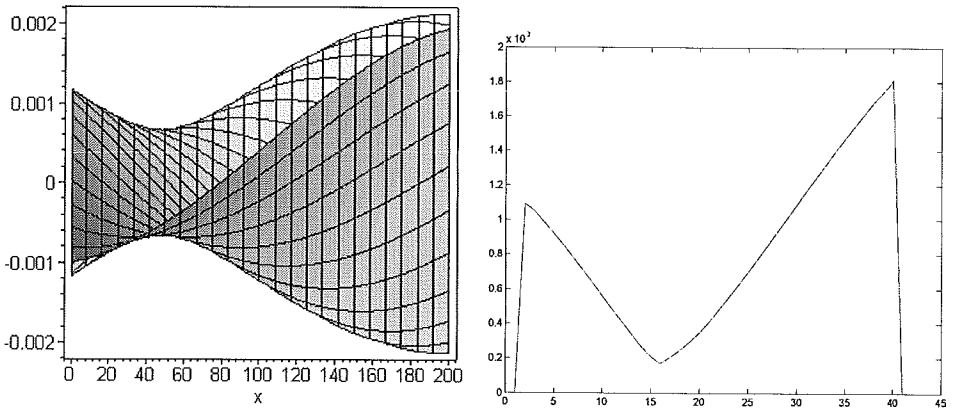

(a) Free surface envelope: analytical

(b) Free surface envelope: numerical

Figure 7: Envelope: combined locked incoming wave and free reflected wave

Although the formats in which the analytical and numerical results are presented are different, it can easily be seen that the numerical result is not correct. The location of the lowest point in the envelope is too far to the right at approximately 120 m from the closed right boundary. In the analytical solution we find this location at approximately 150 m from the closed boundary. Furthermore, the amplitude of the envelope is too small at this location $2 \cdot 10^{-4}$ m where the analytical solution has an amplitude of close to $8 \cdot 10^{-4}$ m. The results of section 2.1 show that the differences between analytical and numerical solutions are not likely to be due to reflections of outgoing waves at the left boundary. It is therefore expected that there are other causes (different from the reflection of the locked waves at the right boundary) that generate free waves in the domain.

5 Concluding remarks

With respect to the wave forces we can state that all differences between the numerical and analytical solution will generate undesired free waves in the model. After eliminating the problems with the irregular structure of the numerically generated wave forces described in section 3.2, we had hoped that the biggest of our problems would be solved. The results of the test given in the last section however, show that there are other causes for the generation of spurious free waves. The boundary conditions have shown to perform almost perfectly for (perpendicularly) outgoing free waves as was shown in the test cases given in section 2.1. We therefore do not expect our problem to be related with the transparency of the boundaries. In our opinion the cause must be found in the generation of the incoming locked wave at the boundary. Since the weakly-reflective boundary conditions developed in this project do not allow locked waves to leave the domain we could not find a test in which only locked waves can be studied.

References

Dongeren, A.R. van, and Svendsen, I.A. 1997. Absorbing-generating boundary conditions for shallow water models. *J. Waterway, Port, Coastal and Ocean Eng., 123(6), pp.303-313.*

Petit, H.A.H., Klopman, G. and Battjes, J.A. 2000. Weakly reflective boundary conditions for the use in a 2D surf beat model. *Report 10-00 Delft. Univ. of Techn., Fac. of Civil Eng. and Geosc., Fluid Mech. Section, Delft.*

Petit, H.A.H., Klopman, G. and Battjes, J.A. 2001. Modified boundary conditions and field equations for a 2D surf beat model. *Report 03-01 Delft. Univ. of Techn., Fac. of Civil Eng. and Geosc., Fluid Mech. Section, Delft.*

Reniers, A.J.H.M., Roelvink, J.A. and van Dongeren, A.R. 2000. Morphodynamic response to wave group forcing. *Proc.* 27^{th} *Int. Conf. Coastal Eng.* , Sydney, Australia.